

Laser-Guided Assembly of Heterotypic Three-Dimensional Living Cell Microarrays

G. M. Akselrod,* W. Timp,[†] U. Mirsaidov,* Q. Zhao,* C. Li,[†] R. Timp,* K. Timp,* P. Matsudaira,[†] and G. Timp*

[†]Beckman Institute, University of Illinois at Urbana-Champaign, Urbana, Illinois 61801; and [†]Whitehead Institute, Massachusetts Institute of Technology, Cambridge, Massachusetts

ABSTRACT We have assembled three-dimensional heterotypic networks of living cells in hydrogel without loss of viability using arrays of time-multiplexed, holographic optical traps. The hierarchical control of the cell positions is achieved with, to our knowledge, unprecedented submicron precision, resulting in arrays with an intercell separation <400 nm. In particular, we have assembled networks of Swiss 3T3 fibroblasts surrounded by a ring of bacteria. We have also demonstrated the ability to manipulate hundreds of *Pseudomonas aeruginosa* simultaneously into two- and three-dimensional arrays with a time-averaged power <2 mW per trap. This is the first time to our knowledge that living cell arrays of such complexity have been synthesized, and it represents a milestone in synthetic biology and tissue engineering.

INTRODUCTION

Synthetic biology is striving to create artificial gene networks to program new cell behaviors (1). And so, the functionality of a cell is being co-opted for the mass production of proteins, the development of new therapeutic drugs, biochemical and environmental sensing, and even computation (1–9). But cells change the pattern of genes they express in response to signals from the environment. In eukaryotes, the extracellular environment plays a vital role in tissue development, differentiation, migration, and cancer. For example, the microenvironment in which cancerous tumor cells reside changes during tumorigenesis (10). At the molecular level, tumorigenesis translates to different signaling requirements during various stages of growth. Therefore, controlling the environment that fosters and supports tumorigenesis is vital for developing therapies for treating the parasitic growth of a tumor (10); and like eukaryotes, bacteria show evidence of the use of intercellular signaling to coordinate multi-cellular activity. For example, “quorum sensing” is a type of communication that requires a sufficient number of bacteria in the local environment to secrete a molecular signal, triggering the expression of target genes (11–15). And finally, whereas some cell types express tissue-specific features in a two-dimensional (2D) culture system, it is apparent that a three-dimensional (3D) environment is required by others (16–24). So, to fully exploit synthetic biology and elicit more complex behavior, the microenvironment of the cell has to be harnessed by emulating the social context and the extracellular matrix.

Living cell microarrays, assembled using optical tweezers in a synthetic hydrogel matrix, may provide a suitable

platform for exploiting the functionality of the cell. Pioneering work by Ashkin demonstrated that optical tweezers could displace and levitate bacteria and viruses (25–29). We show here that it is now possible to create heterotypic microarrays of living cells using optical traps for hierarchical control of the cell positions. We can manipulate hundreds of cells simultaneously with submicron precision into 2D and 3D arrays without loss of viability. The cells are positioned using a time-shared holographic array of 3D optical traps produced through a novel combination of two diffractive elements, a spatial light modulator (SLM) and acoustooptic deflectors (AODs). Although optical trapping allows for the creation of complex networks of cells resembling tissue, the trapping beam must be held on the cells to maintain the array. To fix the position of the cells permanently, we have supported the organized array with a biocompatible scaffold made from a photopolymerizable polyethylene glycol diacrylate (PEGDA) hydrogel. PEGDA hydrogels are especially efficacious as a scaffold because the polymerization time can be relatively short (~3 s) (30). PEGDA hydrogels are also pliable, allowing for transport of nutrients to the cell and waste away from it; and they have demonstrated biocompatibility. Using photopolymerizable hydrogels (30–33), we have immobilized various cell types without loss of viability.

This is the first time that permanent, living cell arrays of such complexity have been synthesized to our knowledge. Previously, holographic arrays of optical traps have been used to permanently arrange up to nine *Escherichia coli* in gelatin (34,35), but the viability of the bacteria was not demonstrated. The extraordinarily long trapping time required to fix the position of a cell in gelatin (~60 min) will adversely affect the viability. Others (30,32,36) have recently demonstrated living cell arrays with positional control from millimeters down to 50 μm using photolithography or dielectrophoretic forces to form patterns of cells within a hydrogel, but they lack direct control over the density, cell

Submitted February 27, 2006, and accepted for publication July 20, 2006.

Address reprint requests to Greg L. Timp, University of Illinois at Urbana-Champaign, Dept. of Electrical and Computer Engineering, 3311 Beckman Institute, 405 N. Mathews Ave. MC-251, Urbana, IL 61801. Tel.: 217-244-9629; E-mail: gtimp@uiuc.edu.

W. Timp, C. Li, and P. Matsudaira's present address is Whitehead Institute, Massachusetts Institute of Technology, Cambridge, MA 02142.

© 2006 by the Biophysical Society

0006-3495/06/11/3465/09 \$2.00

doi: 10.1529/biophysj.106.084079

type, and positioning of individual cells. In contrast, we have assembled hundreds of cells into 2D and 3D heterotypic arrays permanently in a hydrogel scaffold and unequivocally demonstrated viability by measuring membrane integrity, protein production, and metabolic activity. Moreover, the stringent accuracy and submicron precision of the cell placement that we achieve with optical trapping, which is preserved in the low molecular weight hydrogel, is an essential requirement for penetrating stochastic biological processes normally buried by bulk (ensemble) measurements (72). Thus, these complex arrays represent a new tool for the study of gene expression in live cells, affording rigorous control over the 3D microenvironment of the cell.

EXPERIMENTAL DETAILS

Networks of living cells were assembled with time-multiplexed arrays of optical tweezers formed using a novel combination of two diffractive elements, an SLM and AODs, in conjunction with various objectives in an inverted optical microscope (Axiovert 200; Zeiss, Thornwood, NY), as illustrated in Fig. 1. Two different color lasers were used to form the optical traps: a 20-W argon ion laser operated single line at 514 nm; and a continuous wave (CW) TiSi laser, tunable from $\lambda = 850\text{--}900\text{ nm}$ —neither adversely affected viability for the conditions described below.

Multiple time-multiplexed traps were generated in 3D by using a combination of AODs (AA-Optoelectronic, Orsay Cedex, France) and an SLM (Hamamatsu X8267; Hamamatsu City, Japan), which were each optimized for maximum diffraction efficiency at the wavelength of interest. A beam is deflected transverse to the direction of propagation using two orthogonally mounted AODs to give independent control of the x - and y -positions of a trap, allowing for the creation of a 2D network of traps. The beam is time shared between different positions in the 2D array; i.e., it is scanned rapidly from one trap position to the next, dwelling at the desired position in the array just long enough to illuminate an optical trap and fix the location of the cell. When the AOD deflects the beam to the next trap location in the array, cells that are not illuminated will diffuse from the target location and disperse. To prevent dispersal, the rate of deflection between trap positions is properly chosen relative to the time the cell spends in the dark. The maximum allowable dark time depends on the diffusivity of the cell, the size of the array, the scan rate, and the dwell time (38). The laser beam was deflected between trap positions at 100 kHz or 10 μs between traps. The dwell time of the trap over a particular position is variable but is at least 10 μs .

Relay lenses were used to project the 2D array onto an SLM to create a 3D array. The SLM is an optically addressed nematic liquid crystal device configured to act as a phase hologram, using 256 gray levels. It has near-VGA resolution without sharp pixilation, which gives first-order diffraction efficiencies of $\sim 40\%$. Effectively, the SLM was used to

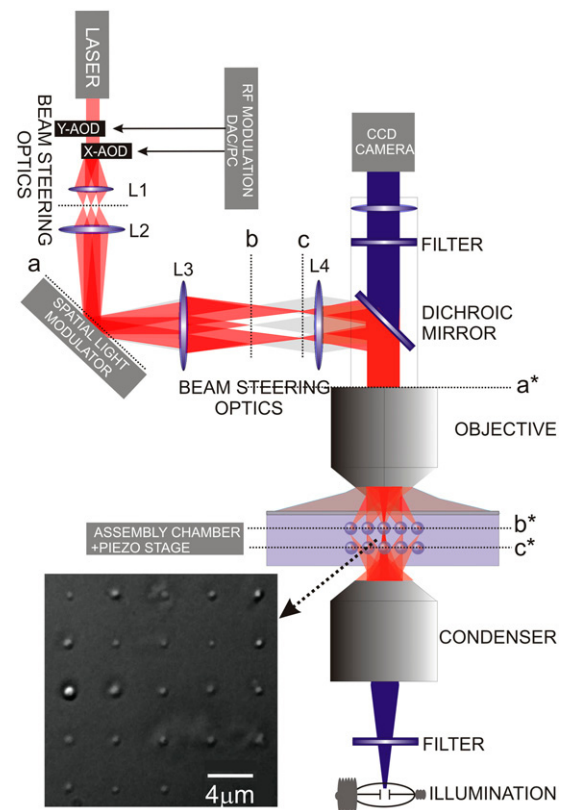


FIGURE 1 Schematic diagram of a time-shared holographic optical trapping apparatus. Trap arrays are formed using a high NA objective in a commercial optical microscope in conjunction with two AODs and an SLM to produce a time-shared (3D) array of optical traps. The plane of the SLM, a , is imaged into the microscope OEA, a^* , and the corresponding planes b and c are imaged into the focal region of the microscope. The same microscope that is used to produce the cell traps is also used for viewing (via the blue beam). The inset in the lower left shows an example of a 2D 5×5 array of *P. aeruginosa* formed using this apparatus and subsequently embedded in hydrogel. The distances are AODs–L1 = 165 mm; L1–L2 = 650 mm; L2–SLM = 332 mm; SLM–L3 = 421 mm; L3–L4 = 1400 mm; and L4–OEA = 493 mm, where the focal lengths are L1 = 150 mm, L2 = 500 mm, L3 = 1000 mm, and L4 = 400 mm.

introduce phase shifts to implement a diffraction grating, offsetting the array transverse to the beam, and Fresnel lenses to offset the array along the optical axis.

The novel combination of an SLM with AODs has practical implications for assembling large arrays of living cells. Ostensibly, a time-multiplexed strategy might preserve cell viability by minimizing beam exposure and the ensuing photodamage. Minimizing the photodamage is a prerequisite for producing viable living cell microarrays. It has been proposed that photodamage in the trap beam results from local heating (39), two-photon absorption (40,41), and photochemical processes leading to the reactive chemical species (42–46). Using temperature-sensitive dyes in micron-scale liposomes, Berns and co-workers (59) have eliminated local heating by a tightly focused CW laser as a photodamage mechanism. Berns measured a temperature

rise of only 1.25°C per $10^7\text{W}/\text{cm}^2$ at $\lambda = 1064$ nm. On the other hand, Block showed that *E. coli* viability depends crucially on wavelength (44)—a change of 20 nm in the wavelength from 850 to 870 nm can affect the lethal dose by a factor of 3. To diminish damage, lasers in the near-infrared band are usually employed since a “biological window” for light exists in tissue (47) for near-infrared wavelengths 700–1500 nm. Light attenuation is governed primarily by scattering processes there (48).

We hypothesize that minimizing the duration of exposure to the beam by time-multiplexing the optical trap will preserve viability (possibly even at shorter wavelengths). Although continuous wave computer-generated holographic optical traps can be formed using an SLM (49–50), the dynamical control required for time-multiplexing optical traps is limited by the slow refresh rate. A dynamic array can be created by encoding different holographic patterns into a reconfigurable SLM and time sharing between patterns. But slow switching times characteristic of nematic liquid crystals (~ 12 Hz for the Hamamatsu) slows the refresh rate of the SLM. Therefore, the switching speed of the SLM affects the light/dark time spent on each dielectric comprising the array, which in turn limits the number of elements in the array and potentially affects photodamage. The switching speed also adversely affects the time required to steer dielectrics elements into an array since the speed of the particle’s movement is not limited by the depth of the trap (relative to the Stokes drag). These constraints, combined with the relatively low diffraction efficiency (40%) and incident power limitations, may adversely affect the size and complexity of the array. In contrast with the SLM, AODs have a high diffraction efficiency ($>70\%$) and permit high-speed (~ 100 kHz) dynamic control over the position of individual cells in an array while minimizing exposure to the beam. And due to the stability of the AODs, the position of each trap can be controlled with ± 19 nm precision.

So, we used the AODs to time-multiplex the position of the optical traps in a 2D array to take full advantage of the high-speed dynamics while encoding a static phase grating on the SLM to introduce additional spatial variations in intensity (required to produce 3D arrays, for example). To determine the phase distribution in the SLM plane (plane *a* in Fig. 1) required to produce the desired intensity distribution in the trapping plane, we used the Gerchberg-Saxton (GS) algorithm (51). The GS algorithm, implemented in LabView 7.1 on a standard Pentium4 PC, uses an iterative technique to find a phase distribution that transforms a light field in transverse plane *a* in Fig. 1 into the desired intensity distribution I_b^0 in another plane *b* in the far field. Starting with a beam with an intensity profile I_a with a uniform phase in plane *a*, which corresponds to a complex amplitude A_a , the complex amplitude of the beam at plane *b* is simply the Fourier transform. If the intensity distribution at *b*, namely $I_b = |A_b|^2$ is not the desired I_b^0 , then the intensity distribution at *b* is replaced by I_b^0 without adjusting the phase in the plane

of *b*. This change affects A_a —the inverse Fourier transform of A_b —and so the intensity distribution at *a* is no longer I_a . The intensity at *a* is subsequently replaced with the actual beam profile while retaining the new phase, and then the procedure iterates until it converges on the phase distribution at *a* that transforms the input beam with intensity I_a in plane *a* through a phase hologram to an approximation of I_b in plane *b*.

Relay lenses were used to image the pattern emerging from the SLM onto the back aperture of the objective. The optical systems comprised of lenses L1 and L2, and L3 and L4 are both afocal; i.e., a collimated incoming beam will emerge collimated. The focal length of the lenses L1, L2, L3, and L4 and the separation between them are chosen so that a small deflection of the beam by the AOD results in a change only in the direction of the laser beam at the objective entrance aperture (OEA), without any change in position (52). Typically, the trapping was done $5\ \mu\text{m}$ from the surface of the coverslip to minimize spherical aberrations from the aqueous media.

Three types of cells were incorporated into microarrays: two rod-shaped bacteria, *Pseudomonas aeruginosa* and *E. coli*, and mouse fibroblasts, Swiss 3T3. *P. aeruginosa* is a gram-negative pathogen. Desiccated *P. aeruginosa* obtained from ATCC (Manassas, VA) (ATCC No. 17468) were rehydrated in a *P. aeruginosa* selective broth (Fisher, Loughborough, Leicestershire, UK; No. MHA000P2P). The bacteria were cultured at a temperature of 26°C and passaged every 1–2 days. Samples were prepared by mixing $200\ \mu\text{L}$ of bacteria solution with $800\ \mu\text{L}$ of $1\times$ phosphate buffer saline (PBS) and centrifuging at $10,000\times g$ rpm for 15 min. The supernatant was aspirated, and the pellet resuspended in 1 mL PBS to remove cellular debris and dead bacteria from the sample solution. The samples contained ~ 5000 bacterium/ μL .

E. coli (DH5 α) was transformed with the plasmid pFNK-203 (3739 basepairs) to express the luxR gene of *Vibrio fischeri* following Weiss et al. (53). The bacteria were plated on LB+Kan and samples grown at 37°C in M9 minimal media (0.2% casamino acids, $200\ \mu\text{M}$ thiamine, 1 mM MgSO_4 , $100\ \mu\text{M}$ CaCl_2) with antibiotics ($50\ \mu\text{g}/\text{ml}$ kanamycin) until the log-growth phase is reached showing an $\text{OD}_{633} = 0.3$. The plasmid incorporated into the *E. coli* contains the lux operon, exerting positive control on the synthesis of a variant of the green fluorescent protein (GFP (LVA)) in response to an acryl-homoserine lactone (AHL) signal. AHL diffuses through the cell membrane and is bound by LuxR, an AHL-dependent transcriptional regulator that activates the expression of *Lac* repressor. We found that AHL concentrations of 7–10 nM induce detectable amounts of GFP-LVA. The LVA tag on the C-terminal end of the GFP marks it for proteolytic digestion. With a half-life of ~ 40 min, the intensity of green fluorescence will diminish without constant production (54).

The Swiss 3T3 (ATCC No. CCL-92) were cultured at 37°C and 5% CO_2 in Dulbecco’s Modified Eagle’s Medium with 10% fetal bovine serum and 1% penicillin/streptomycin.

Mammalian cell samples were created by first detaching cells from the flask surface with a .05% trypsin/EDTA solution. The resulting solution was spun at $5000 \times g$ for 5 min, and the cells were resuspended at a concentration of 400 cells/ μL in PBS.

To impede cell adhesion to the surface, we deposited a polyelectrolyte multi-layer on the culture dishes following Berg et al. (55). Briefly, MatTek (Ashland, MA) dishes were treated with polyallylamine hydrochloride at acidic pH. The dishes were then treated with alternating solutions of polyacrylic acid and polyacrylamide for a total of six layers. Finally, the dishes were baked overnight at 80°C to thermally cross-link the polyelectrolytic layers. This treatment effectively prevents protein adhesion to the surface and inhibits cell adhesion.

Though optical trapping allows for complex and precise assembly of cellular arrays, it is still impractical for long-term experiments. Over time, constant exposure to the laser beams may prove harmful to living cells. Trapping also requires that the array be kept on the optical trapping setup at all times, which limits its portability. To solve these problems, we used a hydrogel matrix prepared from PEGDA. This gel only requires a short (<10 s) burst of ultraviolet (UV) light to polymerize, which limited the amount of time the cells were held in the trap.

To form the hydrogel, we used a prepolymer mix consisting of polyethylene glycol diacrylate (molecular weight = 400) mixed with HEPES-buffered saline to make a 20% (v/v) solution. This solution was combined with the cell suspension to create the final desired concentration of PEGDA. The photoinitiator 2-hydroxy-2-methylpropiophenone (Sigma, St. Louis, MO; No. 405655) was added to the cell/PEGDA solution to a 0.1% (v/v) concentration immediately before trapping. Finally, the cell/PEGDA suspension was pipetted onto MatTek dishes and placed on the microscope. After the array was assembled, the prepolymer solution was exposed to light from a filtered 100-W Hg lamp to form the gel. A beam of UV light in the band $\lambda = 360 \pm 20$ nm with a waist of 2.1 mm and a total power of 6–7 mW was stop-down to a 600- μm diameter spot that exposed the hydrogel for 3–5 s. The exposure was minimized to ensure clonal efficiency and avoid cell damage. We found that cell proliferation was

adversely affected for UV exposures >20 s. The hydrogel was able to adhere to the polyelectrolyte layers due to the acrylate base of both chemistries.

To explicitly illustrate the 3D aspects of the microarrays fixed in hydrogel, samples were imaged using a laser scanning confocal microscope (Leica SP2; Leica Microsystems, Wetzlar, Germany) with a $63\times$, 1.32-numerical aperture (NA) objective and a pinhole size of 1.001Airy unit. Mammalian cells were stained with Calcein AM and propidium iodide, and bacterial cells with SYTO 9 and propidium iodide. Images were deconvolved with Huygens (SVI, Hilversum, The Netherlands) and isosurfaces constructed with Imaris software (Bitplane, Saint Paul, MN). We estimate a typical lateral and axial resolution to be $0.61 \times \lambda/\text{NA} = 235$ nm and $2\lambda/(\text{NA}) = 779$ nm, respectively (2,56).

RESULTS

We first formed living cell microarrays of a prototype cell, *P. aeruginosa*, to evaluate the system performance of the apparatus shown in Fig. 1. Fig. 2 *a* shows the optical system performance, demonstrating the capacity to form a 21×21 2D array of 441 *P. aeruginosa* bacteria formed with a $100\times$, 1.25-NA oil immersion (Zeiss Plan-Apo) objective in a time-shared trap using $\lambda = 900$ nm. The total laser power delivered to the sample was 800 mW, giving a time-averaged power per trap of <2 mW. To our knowledge, this is the largest array of living cells assembled using optical trapping to date. The array was filled either by the diffusion of bacteria into the capture range of a trap or by the use of an additional “shepherd” beam formed with the same laser to move individual bacteria to the trap positions. The maximum size of the array is limited by the dark time, by the diffusion of the cell from the area of the trap, by the objective, and by the laser power delivered through it.

The minor axis of the rod-shaped bacteria ($\sim 1 \mu\text{m}$) is close to the size of the diffraction-limited laser spot, which means that bacteria in the array can be brought nearly into contact. To test the positional control over the cells in the array, we reduced the intercell spacing until the array collapsed. Fig. 2, *b* and *c*, shows laser scanning confocal

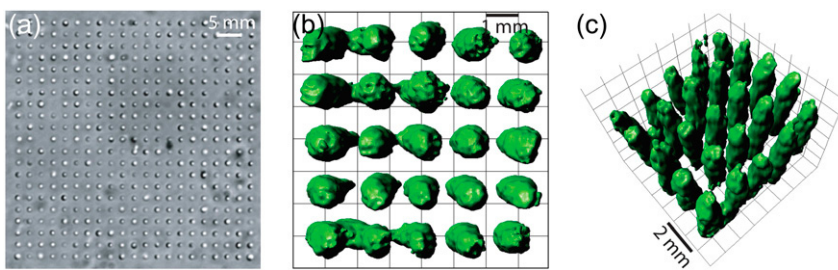


FIGURE 2 Optical micrographs showing 2D microarrays of *P. aeruginosa* bacteria. (a) A transmission micrograph of a 21×21 2D microarray of *P. aeruginosa* formed with a $100\times$, 1.25-NA oil immersion (Zeiss Plan-Apo) objective at $\lambda = 900$ nm using <2 mW per trap. (b) A false-color isosurfaces were generated from volumetric data obtained from deconvolved confocal images of a 5×5 microarray of *P. aeruginosa* assembled with a $100\times$, 1.3-NA oil immersion (Zeiss Plan-Apo) objective at $\lambda = 514$ nm using <2 mW per trap, and embedded in hydrogel. The average center-to-center distance is $1.52 \pm 0.06 \mu\text{m}$ and the average space between each bacterium is 354 ± 134 nm. (c) A 3D representation of (b).

images of a 5×5 2D array formed using 514 nm light with a time-averaged power per trap of <2 mW to ensure viability (see Supplementary Material Fig. 1). This array has a spatial period of $1.52 \pm 0.06 \mu\text{m}$ with a separation between cells of only 354 ± 134 nm on average. This is the first time, to our knowledge, that living cells have been assembled into a pattern with such high resolution. Below a period of $1.1 \mu\text{m}$ with 370 nm between the bacteria, the array tends to collapse, presumably because of limitations associated with the intensity profile in the trap at a power <2 mW. We have found that it is possible to produce an array with a $0.7\text{-}\mu\text{m}$ period using longer wavelength light $\lambda = 900$ nm with a time-averaged power per trap of <15 mW, but viability is compromised for powers >9 mW (see Supplementary Material Fig. 2). These observations suggest that the mode structure of the beam (not the wavelength) used to form the trap and the local electromagnetic environment presented by multiple bacteria in such close proximity may affect the minimum separation that can be maintained.

Using this apparatus, trap arrays are not limited to planar configurations. If the beam entering the objective lens is slightly divergent, then the entire pattern of traps comes to focus at a different point along the optical axis (57). This divergence can be introduced using a Fresnel lens encoded into the phase grating of the SLM. This functionality can be implemented by adding the phase modulation associated with the lens to the existing phase grating computed for the desired 2D pattern so that plane *a* in Fig. 1 can be imaged to planes *b* and *c* at the same time. We have tested this idea with $1\text{-}\mu\text{m}$ diameter latex microspheres and determined that an out-of-plane motion $>\pm 10 \mu\text{m}$ is easily accessible.

Fig. 3 shows a 3D array comprised of three overlapping 2D 5×5 arrays of *P. aeruginosa* separated along the optical axis by $3 \mu\text{m}$ and fixed in hydrogel. The array was formed with a $100\times$, 1.3-NA oil immersion (Zeiss Plan-Apo) objective at $\lambda = 514$ nm using <1 mW time-average power per trap. In the transmission optical micrograph shown in Fig. 3 *a*, the corner vertex of each of the three arrays is highlighted by a (*blue*, *green*, and *red*) circle. Notice that the three arrays are shifted by $4 \mu\text{m}$ along both the *x* and *y* axes to facilitate imaging. The 3D nature of the array is indicated by the focus conditions. The camera focal plane is coplanar with the central (*green*) array so that the top array (*blue*), which is underfocused, appears bright in the image, whereas the underfocused bottom array (*red*) appears dark. However, the transmission micrograph is an ambiguous illustration of the 3D hierarchy within of the array. On the other hand, the false-color isosurfaces reconstructed from confocal images of the same array, shown in Fig. 3, *b–d*, illustrate unequivocally the top (*blue*), middle (*green*), and bottom (*red*) arrays separated by $3 \mu\text{m}$. From the confocal images, we observe that multiple bacteria frequently populate the same trap unless they are loaded carefully—one at a time.

To elicit tissue-specific features, the microarray should mimic not only the 3D character of tissue, but also the hetero-

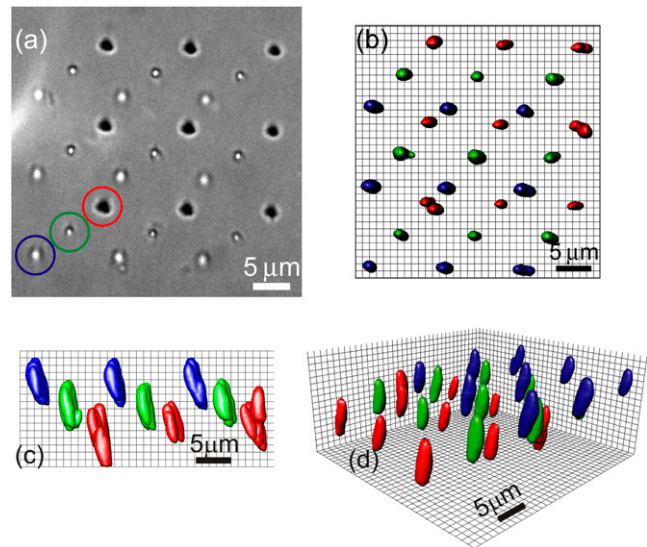


FIGURE 3 A $3 \times 3 \times 3$ 3D array of *P. aeruginosa* bacteria. (*a*) A transmission micrograph of three overlapping 3×3 arrays of *P. aeruginosa*, shifted by $3 \mu\text{m}$ from each other along the optical (*z*) axis and embedded in hydrogel. The arrays are formed with a $100\times$, 1.3-NA oil immersion (Zeiss Plan-Apo) objective using 514 nm light with <1 mW per trap. The corner vertex of each of the arrays is highlighted by a blue, green, and red circle in the figure. The focus is coplanar with the middle of the three arrays so that the underfocused top array (*blue*) appears bright and the overfocused bottom array (*red*) appears to be dark relative to the center array (*green*). The three arrays are shifted by $4 \mu\text{m}$ along both the *x* and *y* axes to facilitate imaging. (*b*) A false-color isosurface, reconstructed from volumetric data obtained from a series of confocal images, showing the offset along the *x* and *y* axes with the *xy*-projection. (*c*) Reconstructed (false color) isosurface *xz*-projection, illustrating the $3\text{-}\mu\text{m}$ separation along the *z* axis. (*d*) A false-color isosurface perspective reconstruction illustrating the top (*blue*), middle (*green*), and bottom (*red*) arrays separated by $2 \mu\text{m}$.

typic microenvironment of the cell. For example, heterotypic systems are needed to model cell-type-specific responses to infection by *P. aeruginosa* (58). Several methods (59–61) have already been explored for coculturing different cell types onto a single substrate in 2D that involve patterning resists that allow cells to attach only to selected regions of a substrate. A second cell type is subsequently attached once the resist is removed to reveal the underlying surface.

Using arrays of time-shared, holographic optical traps, we have assembled 3D, heterotypic living cell microarrays in hydrogel without loss of viability while accounting for variations in the size of the cells. We explored two strategies for trapping large mammalian cells: 1), assigning a high-power single trap to each cell regardless of size, or 2), dedicating an array of low-power multiple traps to each cell where the number of beams in the array is determined by the cell size. Although both strategies can be used successfully, the latter avoids photodamage of a disproportionately small cell due to high power. Fig. 4 *a* shows a homotypic, 2D array of nine trapped Swiss 3T3 fibroblasts with only one trap assigned to each cell. The traps were formed using a Zeiss Neo-Fluor $40\times$, 0.9 NA objective at $\lambda = 514$ nm with a

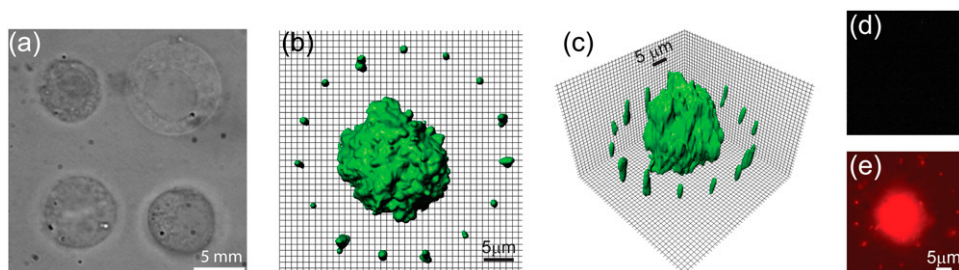


FIGURE 4 Heterotypic microarray of Swiss 3T3 mouse fibroblast and *P. aeruginosa* bacteria. (a) Swiss 3T3 mouse fibroblasts trapped in a 3×3 2D array formed at $\lambda = 514$ nm using a $40\times$ objective with 20 mW per trap. (b) A false-color isosurface reconstruction obtained from a confocal image of a Swiss 3T3 cell trapped with $100\times$ objective using 9–2 mW beams at $\lambda = 900$ nm, surrounded by a ring of 16 *P. aeruginosa*

with each bacterium trapped using a single 2-mW beam. This image was obtained by exciting SYTO 9 labels with 488 nm. (c) The same microarray as in *b* rotated to reflect the 3D aspects of the array. (d and e) Viability assay of the same heterotypic microarray showing an image obtained by exciting propidium iodide labels with 488 nm. The lack of red fluorescence in *d* indicates viability, but after killing the cells with ethanol the fluorescence is intensely red (*e*).

time-averaged power per trap at the sample of 20 mW. In contrast, the heterotypic array comprised of 3T3 fibroblast and 16 *P. aeruginosa* bacteria shown in Fig. 4, *b* and *c*, was formed using $100\times$, 1.3-NA objective at $\lambda = 900$ nm with multiple (9) 2-mW beams trapping the mammalian cell, whereas only a single 2-mW beam was dedicated to each bacterium. The confocal images shown in Fig. 4, *b* and *c*, which were taken ~ 4 h after the formation of the hydrogel, explicitly demonstrate the facility we have for simultaneously assembling cells of differing sizes and types into an arbitrary 3D array. Apparently, because of the small mesh size associated with polyethylene glycol of this molecular weight (2–7 nm (47)), the position of the cells is rigidly fixed within the array. This is the first time, to our knowledge, that a permanent, heterogeneous network of cells has been assembled with such precision. Notice that the bacteria are encircling the waist of the 3T3 cell, imitating the onset of infection. According to Rocha et al. (62) infection is supposed to begin with the adherence of *P. aeruginosa* to host cells through pili and nonpili mechanisms (56,61). Living cell microarrays may provide an opportunity to study infection through control of colonization and the biochemical library in the microenvironment of a cell.

Generally, for every cell type that we manipulate into an array in hydrogel, we have to assess the following: 1), photodamage (39–41,64), 2), cytotoxicity/cytocompatibility of the photoinitiator (48), and 3), biocompatibility in the hydrogel. The viability of the cells in this array was assessed using two nucleic acid stains: SYTO9 and propidium iodide. SYTO9 permeates the membrane of a living cell and labels nucleic acids with green fluorescence, whereas membrane-impermeant propidium iodide labels the nucleic acids of membrane-compromised cells with red fluorescence. Fig. 4, *b* and *d*, illustrates the results of the assay; i.e., the bright green fluorescence shown in Fig. 4 *b* observed in conjunction with a lack of red fluorescence in Fig. 4 *d* indicates that both cell types remain viable. However, after exposure of the same cells to ethanol, the fluorescence is intensely red as shown in Fig. 4 *e*.

Although assays of viability using these dyes have been found to correspond to $\sim 90\%$ clonal efficiency (65,66), they only measure membrane integrity. We want to assess viability of the optically patterned, hydrogel-encapsulated

cells as a function of time. To facilitate a comparison to previous characterizations of the photodamage caused by optical trapping on *E. coli* metabolism (66,67), we monitored protein production directly by observing the production of GFP in response to chemical induction using an AHL signal. Fig. 5 *a* shows a transmission micrograph of a 5×5 2D array of *E. coli* bacteria formed in hydrogel with a $100\times$, 1.25-NA oil immersion (Zeiss Plan-Apo) objective in a time-shared trap using $\lambda = 900$ nm, taken immediately after gelation. (The time-averaged power per trap was < 2 mW.) The array is then incubated at room temperature. After 37 h, we induced GFP production with 500 nm AHL, and we observe green fluorescence 5.5 h later. Fig. 5 *b* shows the green fluorescent signal obtained from the same array after exposure to 500 nm of AHL, 43 h after assembly using 470 nm excitation. Every element of the array is fluorescing green, indicating that every cell is producing GFP(LVA). Also notice that the position of each cell in the array has not changed after 43 h, indicating that the bacteria have been immobilized.

The fluorescence induced up to 43 h after fixing the array is an unambiguous measure of protein production and metabolic activity in the bacteria, and the perfect viability of the

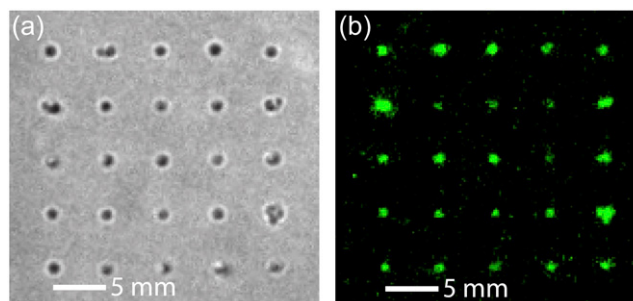


FIGURE 5 A 5×5 2D array of *E. coli* bacteria incorporating the receiver plasmid pFNK-203. (a) A transmission micrograph of a 5×5 array of *E. coli* embedded in hydrogel. The array is formed with a $100\times$, 1.3-NA oil immersion (Zeiss Plan-Apo) objective using $\lambda = 900$ nm using < 2 mW per trap. (b) A green fluorescent image of the same array obtained using 470 nm excitation, after inducing the production of GFP within the *E. coli* with 500 nm of AHL 43 h after gelling. Every element of the array is fluorescing green. These images indicate metabolic activity and cell viability up to 43 h after fixing the array in hydrogel.

elements of the array. For reference, in a minimal media like M9, a culture of this strain (that is not constrained by the hydrogel) doubles about every 2 h, whereas in rich media, a culture doubles every 20–30 min. We have measured protein production, or an operational lifetime, of 48 h after fixing the array in hydrogel. The efficacy of whole cell-based environmental sensors relies on similar measures of the operational lifetime and shelf life (68). For comparison, Kuang et al. (69) recently reported an operational life span of a single cell, *E. coli* genotoxin biosensor of more than 6 h under ambient conditions with a shelf-life of 2 weeks when stored at 4°C.

SUMMARY

It is now possible to assemble hundreds of living cells into 3D heterotypic microarrays with submicron resolution without loss of viability using time-shared, holographic optical traps. In an attempt to preserve cell viability, the optical traps are implemented using a novel combination of two diffractive elements: an SLM and AOD. The viability we observed at $\lambda = 514$ nm and for $\lambda > 850$ nm is an indication of the promise of this strategy. This laser-guided technique is superior to lithographic and dielectrophoresis cell patterning because it offers 3D placement with high precision and selectivity, limited only by the diffusion of the cell during the dark time and photodamage.

The development of living cell microarrays brightens the prospects for synthetic biology and tissue engineering. Although single cells are currently the crucible for synthetic biology, to fully exploit it and elicit more complex regulatory behaviors, the microenvironment surrounding the cell must be harnessed as well. Signals between cells can be transmitted through extracellular space by molecular diffusion, through receptor proteins in the cell membrane, or directly through gap junction proteins that provide a communication link between the cytoplasm of adjacent cells. Cells can acquire positional information by sensing a chemical gradient that is interpreted according to specific genetic instructions, depending on developmental history; or the position could be specified by lateral inhibition in which differentiating cells secrete an inhibitory signaling molecule that acts on the nearest neighbors to prevent them from developing similarly.

The fluorescent array shown in Fig. 5 demonstrates unequivocally the manipulation of gene expression through the broadcast of a biochemical signal. Using the same methods, we should be able to explore gene expression in live cells using only a few signaling molecules at a time by controlling the position of cells transmitting and receiving the signals. Thus, the potential exists for manipulating 3D biochemical gradient communication with physiologically relevant concentrations and gradients using living cell microarrays. More complex microarrays offer a more diverse library of biochemical signals and at the same time afford us stringent control over the 3D microenvironment of every cell in the

array, making it useful in studies of tissue development and differentiation in eukaryotes, as well as cancer.

SUPPLEMENTARY MATERIAL

An online supplement to this article can be found by visiting BJ Online at <http://www.biophysj.org>.

We gratefully acknowledge frequent discussions with G. Spalding, who generously provided us with a software implementation of the Gerchberg-Saxton algorithm. Conversations with L. Schook and R. Weiss stimulated some of our initial work. R. Weiss contributed the pFNK-203 plasmid.

This effort is partially supported by National Science Foundation Nanoscale Interdisciplinary Research Team No. 0404030 and a Beckman Foundation grant.

REFERENCES

- Basu, S., Y. Gerchman, C. H. Collins, F. H. Arnold, and R. Weiss. 2005. A synthetic multicellular system for programmed pattern formation. *Nature*. 434:1130–1134.
- Grabherr, R., E. Nilsson, G. Striedner, and K. Bayer. 2002. Stabilizing plasmid copy number to improve recombinant protein production. *Biotechnol. Bioeng.* 77:142–147.
- Noll, F., M. Sumper, and N. Hampp. 2002. Nanostructure of diatom silica surfaces and of biomimetic analogues. *Nano Lett.* 2:91–95.
- Clark, H. A., S. L. R. Baker, M. Brasuel, M. T. Miller, E. Monson, S. Parus, Z.-Y. Shi, A. Song, B. Thorsud, R. Kopelman, A. Ade, W. Meixner, and others. 1998. Subcellular optochemical nanobiosensors: probes encapsulated by biologically localised embedding (PEBBLEs). *Sens. Actuators B. Chem.* 51:12–16.
- Pancrazio, J. J., J. P. Whelan, D. A. Borkholder, W. Ma, and D. A. Stenger. 1999. Development and application of cell-based biosensors. *Ann. Biomed. Eng.* 27:697–711.
- Belkin, S. 2003. Microbial whole-cell sensing systems of environmental pollutants. *Curr. Opin. Microbiol.* 6:206–212.
- Projan, S. J. 2002. New (and not so new) antibacterial targets—from where and when will the novel drugs come? *Curr. Opin. Pharmacol.* 2:513–522.
- Bray, D. 1995. Protein molecules as computational elements in living cells. *Nature*. 376:307–312.
- Ferber, D. 2004. Synthetic biology: microbes made to order. *Science*. 303:158–161.
- Lim, K.-H., and C. M. Counter. 2005. Reduction in the requirement of oncogenic Ras signaling to activation of PI3K/AKT pathway during tumor maintenance. *Cancer Cell*. 8:381–392.
- Pappas, K. M., C. L. Weingart, and S. C. Winans. 2004. Chemical communication in proteobacteria: biochemical and structural studies of signal synthases and receptors required for intercellular signalling. *Mol. Microbiol.* 53:755–769.
- Miller, M. B., and B. L. Bassler. 2001. Quorum sensing in bacteria. *Annu. Rev. Microbiol.* 55:165–199.
- Whitehead, N. A., A. M. L. Barnard, H. Slater, N. J. L. Simpson, and G. P. C. Salmond. 2001. Quorum-sensing in gram-negative bacteria. *FEMS Microbiol. Rev.* 25:365–404.
- Greenberg, E. P. 2003. Tiny teamwork. *Nature*. 424:134.
- Sauer, K. 2003. The genomics and proteomics of biofilm formation. *Genome Biol.* 4:219.
- Dunn, J. C. Y., M. L. Yarmush, H. G. Koebe, and R. G. Tompkins. 1989. Hepatocyte function and extracellular-matrix geometry—long-term culture in a sandwich configuration. *FASEB J.* 3:174–177.
- Kleinman, H. K., R. J. Klebe, and G. R. Martin. 1981. Role of collagenous matrices in the adhesion and growth of cells. *J. Cell Biol.* 88:473–485.

18. Hay, E. D. 1981. Extracellular matrix. *J. Cell Biol.* 91:S205–S223.
19. Chambard, M., J. Gabrion, and J. Mauchamp. 1981. Influence of collagen gel on the orientation of epithelial cell polarity: follicle formation from isolated thyroid cells and from preformed monolayers. *J. Cell Biol.* 91:157–166.
20. Montesano, R., P. Mouron, M. Amherdt, and L. Orci. 1983. Collagen matrix promotes reorganization of pancreatic endocrine cell monolayers into islet-like organoids. *J. Cell Biol.* 97:935–939.
21. Ingber, D. E., J. A. Madri, and J. D. Jamieson. 1986. Basement membrane as a spatial organizer of polarized epithelia. Exogenous basement membrane reorients pancreatic epithelial tumor cells in vitro. *Am. J. Pathol.* 122:129–139.
22. Hall, H. G., D. A. Farson, and M. J. Bissell. 1982. Lumen formation by epithelial cell lines in response to collagen overlay: a morphogenetic model in culture. *Proc. Natl. Acad. Sci. USA.* 79:4672–4676.
23. Leffert, H. L., and D. Paul. 1972. Studies on primary cultures of differentiated fetal liver cells. *J. Cell Biol.* 52:559–568.
24. Cukierman, E., R. Pankov, and K. M. Yamada. 2002. Cell interactions with three-dimensional matrices. *Curr. Opin. Cell Biol.* 14:633–639.
25. Ashkin, A. 1970. Acceleration and trapping of particles by radiation pressure. *Phys. Rev. Lett.* 24:156–159.
26. Ashkin, A. 1992. Forces of a single-beam gradient laser trap on a dielectric sphere in the ray optics regime. *Biophys. J.* 61:569–582.
27. Ashkin, A., and J. M. Dziedzic. 1989. Optical trapping and manipulation of single living cells using infrared laser beams. *Ber. Bunsen Phys. Chem.* 93:254–260.
28. Ashkin, A., and J. M. Dziedzic. 1971. Optical levitation by radiation pressure. *Appl. Phys. Lett.* 19:283–285.
29. Ashkin, A., K. Schutze, J. M. Dziedzic, U. Euteneuer, and M. Schliwa. 1990. Force generation of organelle transport measured in vivo by an infrared laser trap. *Nature.* 348:346–348.
30. Liu, V. A., and S. N. Bhatia. 2002. Three-dimensional photopatterning of hydrogels containing living cells. *Biomed. Microdevices.* 4:257–266.
31. Mellott, M. B., K. Searcy, and M. V. Pishko. 2001. Release of protein from highly cross-linked hydrogels of poly(ethylene glycol) diacrylate fabricated by UV polymerization. *Biomaterials.* 22:929–941.
32. Koh, W. G., A. Revzin, and M. V. Pishko. 2002. Poly(ethylene glycol) hydrogel microstructures encapsulating living cells. *Langmuir.* 18:2459–2462.
33. Cruise, G. M., O. D. Hegre, F. V. Lamberti, S. R. Hager, R. Hill, D. S. Scharp, and J. A. Hubbell. 1999. In vitro and in vivo performance of porcine islets encapsulated in interfacially photopolymerized poly(ethylene glycol) diacrylate membranes. *Cell Transplant.* 8:293–306.
34. Jordan, P., H. Clare, L. Fiendrig, J. Leach, J. Cooper, and M. Padgett. 2004. Permanent 3D microstructures in a polymeric host created using holographic optical tweezers. *J. Mod. Optic.* 51:627–632.
35. Jordan, P., J. Leach, M. Padgett, P. Blackburn, N. Isaacs, M. Goksor, D. Hanstorp, A. Wright, J. Girkin, and J. Cooper. 2005. Creating permanent 3D arrangements of isolated cells using holographic optical tweezers. *Lab Chip.* 5:1224–1228.
36. Albrecht, D. R., V. L. Tsang, R. L. Sah, and S. N. Bhatia. 2005. Photo- and electropatterning of hydrogel-encapsulated living cell arrays. *Lab Chip.* 5:111–118.
37. Yu, J., J. Xiao, X. Ren, K. Lao, and X. S. Xie. 2006. Probing gene expression in live cells, one protein molecule at a time. *Science.* 311:1600–1603.
38. Molloy, J. E. 1998. Optical chopsticks: digital synthesis of multiple optical traps. *Methods Cell Biol.* 55:205–216.
39. Liu, Y., G. J. Conek, M. W. Berns, and B. J. Tromberg. 1996. Physiological monitoring of optically trapped cells: assessing the effects of confinement by 1064 nm laser tweezers using microfluorometry. *Biophys. J.* 71:2158–2167.
40. Berns, M. W. 1976. A possible two-photon effect in vitro using a focused laser beam. *Biophys. J.* 16:973–977.
41. König, K., H. Liang, M. W. Berns, and B. J. Tromberg. 1996. Cell damage in near-infrared multimode optical traps as a result of multiphoton absorption. *Opt. Lett.* 21:1090–1092.
42. Calmettes, P. P., and M. W. Berns. 1983. Laser-induced multiphoton processes in living cells. *Proc. Natl. Acad. Sci. USA.* 80:7197–7199.
43. Block, S. M. 1990. Optical tweezers: a new tool for biophysics. In *Non-Invasive Techniques in Cell Biology: Modern Review of Cell Biology*, Vol. 9. J. K. Foskett and S. Grinstein, editors. Wiley-Liss, New York. 375–402.
44. Neuman, K. C., E. H. Chadd, G. F. Liou, K. Bergman, and S. M. Block. 1999. Characterization of photodamage to *Escherichia coli* in optical traps. *Biophys. J.* 77:2856–2863.
45. Svoboda, K., and S. M. Block. 1994. Biological applications of optical forces. *Annu. Rev. Biomol. Struct.* 23:247–285.
46. Svoboda, K., and S. M. Block. 1994. Force and velocity measured for single kinesin molecules. *Cell.* 77:773–784.
47. Cruise, G. M., D. S. Scharp, and J. A. Hubbell. 1998. Characterization of permeability and network structure of interfacially photopolymerized poly(ethylene glycol) diacrylate hydrogels. *Biomaterials.* 19:1287–1294.
48. Bryant, S. J., C. R. Nettleman, and K. S. Anseth. 2000. Cytocompatibility of UV and visible light photoinitiating systems on cultured NIH/3T3 fibroblasts in vitro. *J. Biomed. Sci. Polymer Edn.* 11:439–457.
49. Roichman, Y., and D. G. Grier. 2005. Holographic assembly of quasicrystalline photonic heterostructures. *Opt. Express.* 13:5434–5439.
50. Polin, M., K. Ladavac, S.-H. Lee, Y. Roichman, and D. Grier. 2005. Optimized holographic optical traps. *Opt. Express.* 13:5831–5845.
51. Soifer, V. A., V. Kotlyar, and L. Doskolovich. 1997. *Iterative Methods for Diffractive Optical Elements Computation*. Taylor & Francis, London.
52. Fallman, E., and O. Axner. 1997. Design for fully steerable dual-trap optical tweezers. *Appl. Opt.* 36:2107–2113.
53. Weiss, R., and T. F. Knight Jr. 2001. Engineered communications for microbial robotics. In *DNA Computing: 6th International Workshop on DNA-Based Computers, DNA 2000, Leiden, The Netherlands, June 13–17, 2000: Revised Papers*. A. Condon and G. Rozenberg, editors. Springer, Berlin. 1–16.
54. Andersen, J. B., C. Sternberg, L. K. Poulsen, S. P. Bjorn, M. Givskov, and S. Molin. 1998. New unstable variants of green fluorescent protein for studies of transient gene expression in bacteria. *Appl. Environ. Microbiol.* 64:2240–2246.
55. Berg, M. C., J. Choi, P. T. Hammond, and M. F. Rubner. 2003. Tailored micropatterns through weal: polyelectrolyte stamping. *Langmuir.* 19:2231–2237.
56. Pawley, J. B. 1995. *Handbook of Biological Confocal Microscopy*, 2nd ed. Plenum Press, New York.
57. Curtis, J. E., B. A. Koss, and D. G. Grier. 2002. Dynamic holographic optical tweezers. *Opt. Commun.* 207:169–175.
58. Coburn, J., and D. W. Frank. 1999. Macrophages and epithelial cells respond differently to the *Pseudomonas aeruginosa* type III secretion system. *Infect. Immun.* 67:3151–3154.
59. Bhatia, S. N., U. J. Balis, M. L. Yarmush, and M. Toner. 1999. Effect of cell-cell interactions in preservation of cellular phenotype: cocultivation of hepatocytes and nonparenchymal cells. *FASEB J.* 13:1883–1900.
60. Bhatia, S. N., U. J. Balis, M. L. Yarmush, and M. Toner. 1998. Microfabrication of hepatocyte/fibroblast co-cultures: role of homotypic cell interactions. *Biotechnol. Prog.* 14:378–387.
61. Ostuni, E., R. Kane, C. S. Chen, D. E. Ingber, and G. M. Whitesides. 2000. Patterning mammalian cells using elastomeric membranes. *Langmuir.* 16:7811–7819.
62. Rocha, C. L., E. A. Rucks, D. M. Vincent, and J. C. Olson. 2005. Examination of coordinate effects of *Pseudomonas aeruginosa* ExoS on Rac1. *Infect. Immun.* 73:5458–5467.
63. Pier, G. B., M. Grout, and T. S. Zaidi. 1997. Cystic fibrosis transmembrane conductance regulator is an epithelial cell receptor for clearance of *Pseudomonas aeruginosa* from the lung. *Proc. Natl. Acad. Sci. USA.* 94:12088–12093.

64. König, K., H. Liang, M. W. Berns, and B. J. Tromberg. 1995. Cell damage by near-IR microbeams. *Nature*. 377:20–21.
65. Neuman, K. C., Edmund H. Chadd, Grace F. Liou, Keren Bergman, and Steven M. Block. 1999. Characterization of photodamage to *Escherichia coli* induced by optical traps. *Biophys. J.* 77:2856–2863.
66. Ericsson, M., D. Hanstorp, P. Hagberg, J. Enger, and T. Nystrom. 2000. Sorting out bacterial viability with optical tweezers. *J. Bacteriol.* 182:5551–5555.
67. Neuman, K. C., E. H. Chadd, G. F. Liou, K. Bergman, and S. M. Block. 1999. Characterization of photodamage to *Escherichia coli* in optical traps. *Biophys. J.* 77:2856–2863.
68. Bjerketorp, J., S. Hakansson, S. Belkin, and J. K. Jansson. 2006. Advances in preservation methods: keeping biosensor microorganisms alive and active. *Curr. Opin. Biotechnol.* 17:43–49.
69. Kuang, Y., I. Biran, and D. R. Walt. 2004. Living bacterial cell array for genotoxin monitoring. *Anal. Chem.* 76:2902–2909.